Geophys. J. Int. (2000) **141,** 801–808

On the detection and identification of converted and reflected phases from receiver functions

Sébastien Chevrot[1] and Nicole Girardin[2]

[1] *Department of Earth, Atmospheric and Planetary Sciences, Massachusetts Institute of Technology, Cambridge,* MA 02139, *USA. E-mail: chevrot@quake.mit.edu*

[2] *Laboratoire de sismologie, Institut de Physique du Globe,* 4 *Place Jussieu,* 75252 *Paris, cedex* 05, *France*

Accepted 2000 January 31. Received 1999 November 5; in original form 1999 February 8

SUMMARY

We develop a simple methodology to extract information related to crustal structure such as the mean V_P/V_S ratio, the magnitude of lateral variations and the presence of discontinuities from a selection of receiver functions. We show that crustal phases can be detected and exploited on individual receiver functions. Two filtering techniques, based on singular value decomposition and spectral matrix filtering, are proposed to enhance the coherent phases in receiver functions. Additionally, the relative traveltimes and slownesses between the different phases are utilized for a more reliable phase identification. We apply these methods to data of station PRU (Czech Republic) and compare the results with a classical time-domain waveform inversion. We find a good qualitative agreement between the simple crustal models inferred from the two approaches. Waveform modelling suggests that the identification of converted phases can still be ambiguous and other geophysical or geological constraints are needed.

Key words: crustal structure, inversion, Poisson's ratio, seismic phase identification.

1 INTRODUCTION

Teleseismic waves monitored by permanent stations of global seismographic networks contain important information related to the shallow structure beneath these stations. The so-called receiver function analysis, which was introduced by Burdick & Langston (1977) and later improved by Langston (1979), provides an elegant way to determine the crustal structure through time-domain inversion of stacked receiver functions (Owens *et al.* 1984).

These pioneering works stimulated active research in the field, and receiver function studies have been used to address a wide range of geophysical problems. Receiver functions constrain the depth and the shape of the crust–mantle boundary, which is important for a better understanding of the crustal structure and its evolution (Owens *et al.* 1984; Owens & Zandt 1985; Durrheim & Mooney 1991). The Moho thickness is simply estimated from the width of the pulse generated by the *P*-to-*S* conversion at the Moho. The mean V_P/V_S ratio in the crust can be determined from traveltime ratios of crustal phases observed on receiver functions (Zandt *et al.* 1995). Therefore, it is possible to determine the crustal Poisson's ratio that is related to the composition of the lower crust (Christensen 1996). Zandt & Ammon (1995) used this technique to constrain Poisson's ratio in various tectonic regions. Receiver functions can also be used to constrain crustal anisotropy from the joint inversion of radial and transverse components (Kosarev *et al.* 1984; McNamara & Owens 1993; Levin & Park 1997a; Savage 1998). Additionally, receiver functions have been widely used to study the transition zone discontinuities (see Chevrot *et al.* 1999 for a review) and the fine structure of the lithosphere (Bostock 1997, 1998).

Crucial in all these studies is the ability to identify unambiguously the phases in the *P*-wave coda. An important criterion for detection is the coherence of records observed for different distances and backazimuths. In order to minimize the influence of lateral variations, receiver functions are often stacked in narrow distance and azimuth ranges (Owens *et al.* 1984; Owens & Crosson 1988; Cassidy 1992). Yuan *et al.* (1997) used moveout corrections in order to align converted phases on a set of receiver functions. Such corrections can improve the coherence of phases, but the level of noise and the strong lateral variations of the crustal structure can still make the detection and identification of these phases difficult.

The main purpose of this paper is to investigate new methods to detect and analyse crustal phases from receiver functions without stacking. To improve the signal-to-noise ratio on individual traces, two filtering techniques, singular value decomposition (SVD) and spectral matrix filtering (SMF), have been adapted to the processing of receiver functions. The method is applied to seismograms recorded at station PRU (Czech Republic; latitude 49.99°N, longitude 14.54°E). This station provides high-quality records of events that are widely distributed in distance and backazimuth. Moreover,

the crustal and lithospheric structures are fairly well known as a result of systematic explosion seismology investigations (see Beránek & Zátopek 1981 for a review) and the analysis of *P*-wave station residuals (Babuška & Plomerova 1992).

2 ENHANCING CRUSTAL PHASES WITHOUT STACKING

2.1 Data analysis

We first make a careful data selection based on the noise level in the records. The traces with strong *PP* or *PcP* arrivals between 10 and 80 s after the *P* wave are rejected. The three *Z*, *N* and *E* components are rotated to the *L*, *SV* and *SH* axes. *L* is along the *P* principal motion direction, *SV* is in the *P*-wave propagation plane and is normal to *L*, and *SH* is normal to both *L* and *SV* (see Fig. 1). The epicentral backazimuth is used to determine the radial component. An additional rotation is performed with an angle that is calculated from the radial and vertical components correlation matrix (Vinnik 1977). The *L* component is then deconvolved from the horizontal components. The deconvolution procedure suppresses the effects of the source (rupture process, magnitude) and of the wave propagation before the converting interface. After this operation, the resulting *SV* trace, which is called a receiver function, contains all the information related to the *P–SV* conversions at the seismic discontinuities beneath the station. Our technique differs from the method introduced by Yuan *et al.* (1997) by two important points. First, no low-pass filter is applied to the data. We introduce different filtering techniques to preserve the high-frequency phases that arrive in a short (typically less than 15 s) time interval after the direct *P* wave. These techniques enhance the coherent signal observed in the receiver functions and constitute a significant improvement over the simple moving average of adjacent traces used by Yuan *et al.* (1997). Second, the receiver functions are not stacked after moveout corrections. Rather, we look for possible variations of traveltimes with distance (or incidence angle) and azimuth in order to identify crustal phases and to evaluate the lateral variations of the crustal structure in a simple and yet efficient way.

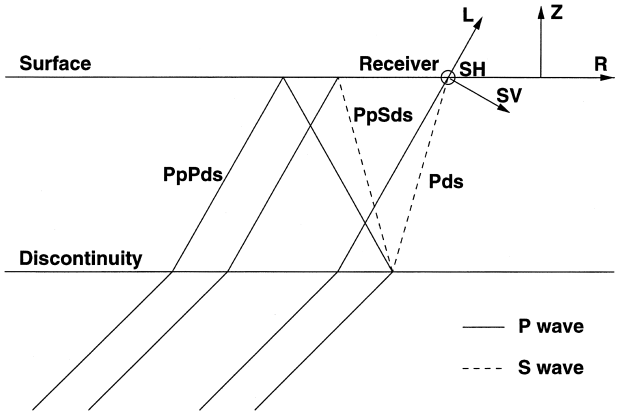

Figure 1. Schematic ray diagram of the *Pds* phase, converted from *P* to *S* at a depth *d* beneath the receiver. Also shown are the first multiple, *PpPds*, transmitted as *P*, reflected from the free surface as *P* and reflected from the discontinuity as *S*, and the second multiple, *PpSds*, transmitted as *P*, reflected from the free surface as *S* and reflected from the discontinuity as *S*. Axis *L* corresponds to the principal direction of the *P*-wave particle motion. Axis *SV* is perpendicular to the axis *L* and is optimum for detecting the *Pds* phases. Axis *SH* is orthogonal to both *L* and *SV*.

After selection and processing, the remaining set of receiver functions for a particular station is called its 'seismic section'. The seismic section for station PRU, made up of a collection of 54 receiver functions with various epicentral distances and backazimuths, is shown in Fig. 2. The receiver functions are sorted as a function of increasing epicentral distance. Converted phases and crustal multiples show a good coherence from one trace to another. In particular, two phases, arriving about 3.0 and 10.5 s after the *P* wave, are clearly detected. The traveltimes of the different phases relative to *P* depend on incidence angle and therefore on epicentral distance. This dependence is clearly seen on the first traces, for which epicentral distances are less than 50°. In this epicentral distance range, the two most energetic phases show apparent slownesses relative to *P* of opposite signs. It will be shown later how such information can help to identify these phases.

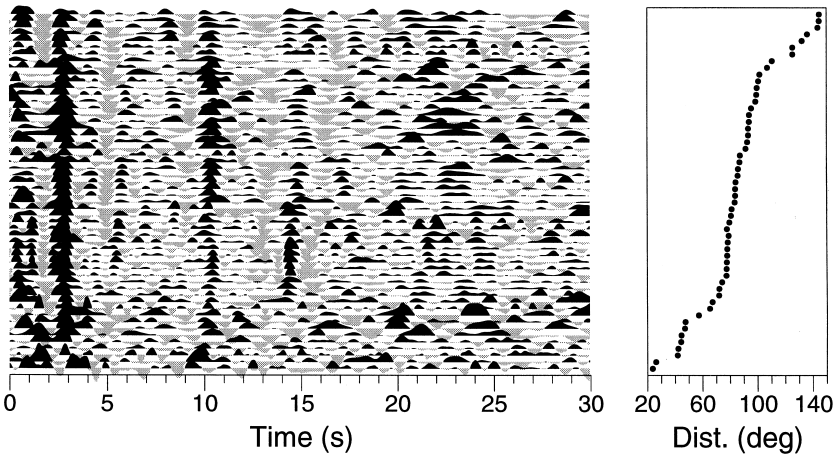

Figure 2. PRU seismic section: *SV*-component receiver functions recorded by station PRU, sorted according to increasing epicentral distances.

2.2 Filtering the receiver functions

In spite of a very careful selection of records, the section shown in Fig. 2 is contaminated by noise. The low-pass filtering of the data to suppress short-period scattered phases, a key factor in detecting successfully *P*-to-*S* conversions at the transition zone discontinuities (Vinnik 1977), is of limited interest for studying crustal phases. Fig. 3 displays the PRU section low-pass filtered at 3 s. Noise is still present in the section, and many coherent phases that were observed on the broad-band section have disappeared. Therefore, some information is lost for little improvement of the signal-to-noise ratio. Filtering techniques that rely on the coherence of signals from one trace to another are preferable. Glangeaud & Mari (1994) give a good overview of these techniques. In the present paper, two different techniques will be discussed: singular value decomposition (SVD) (Freire & Ulrych 1988) and spectral matrix filtering (SMF) (Mari & Glangeaud 1990). These techniques were initially introduced to improve vertical seismic profiling data. The main difference between these two techniques is that SVD gives better results when the seismic phases are aligned on all the records. In practice, aligning reflected and converted phases with moveouts is not a problem (Yuan *et al.* 1997), and this operation is reversible, that is, the traces can be restored to their initial state.

2.2.1 *Singular value decomposition filtering*

SVD filtering is widely utilized in image processing and has been introduced recently in seismic prospecting (Freire & Ulrych 1988). A rectangular $M \times N$ data matrix D is defined by the M receiver functions of N points that belong to the seismic section. The matrix element D_{ij} is the amplitude of the signal on the ith receiver function and for the temporal index j. The singular value decomposition of D is given by

$$D = \sum_{i=1}^{R} \sigma_i \mathbf{u}_i \mathbf{v}_i^{\mathrm{T}} , \tag{1}$$

with R the rank of D, $\mathbf{u}_i$ the ith eigenvector of the matrix DD^{T}, $\mathbf{v}_i$ the ith eigenvector of the matrix $D^{\mathrm{T}}D$ and σ_i the ith singular value of D. The σ_i, ordered by decreasing magnitude, are the eigenvalues of both DD^{T} and $D^{\mathrm{T}}D$, and are always real and positive. The data matrix D can be seen as a superposition of eigenimages $\sigma_i \mathbf{u}_i \mathbf{v}_i^{\mathrm{T}}$. Since the amplitude of the ith eigenimage is proportional to the corresponding eigenvalue σ_i, most of the information is contained in the first few eigenimages. In the absence of noise and if the different seismic phases were coherent on the whole section, the first eigenimage would contain all the signal. When noise is present, it will be recovered on the eigenimages of ranks higher than 1. In practice, waves are not coherent on the complete section but it is still possible to isolate the coherent phases by a truncated sum over eigenimages:

$$D_{\mathrm{fil}} = \sum_{i=1}^{n} \sigma_i \mathbf{u}_i \mathbf{v}_i^{\mathrm{T}} , \tag{2}$$

where $1 \leq n < R$. Eigenimages corresponding to a rank lower than n are dominated by the signal, whereas eigenimages corresponding to a rank higher than n represent noise. With a careful selection of n, it is thus possible to separate the signal space from the noise space. A simple procedure is to examine the shape of the spectrum and to keep all the eigenvalues that are lower than some critical rank, beyond which a regular decrease of the spectrum is observed. Fig. 4 displays the spectrum of the matrix D formed with all the records of Fig. 2. The dominant part of the signal is found on the first 6 eigenimages.

Fig. 5 shows the data for station PRU filtered by SVD with $n = 6$. The incoherent noise has almost disappeared and the section is clearly improved. Note that this filtering technique tends to enhance the spatial–temporal coherence of waves. The true arrival times and amplitudes of waves on individual traces could be recovered if a larger number of eigenimages were kept, but higher-order eigenimages are more severely contaminated by noise. Therefore, a compromise has to be found between the conservation of the signal's complexity and the improvement of the signal-to-noise ratio. SVD filtering gives poor results when the epicentral distance is less than 60°, that is, when the onset of converted or reflected phases varies. For this epicentral distance range, larger variations of the arrival times of the crustal phases are observed. Hence, a larger number of eigenimages would be required to reproduce

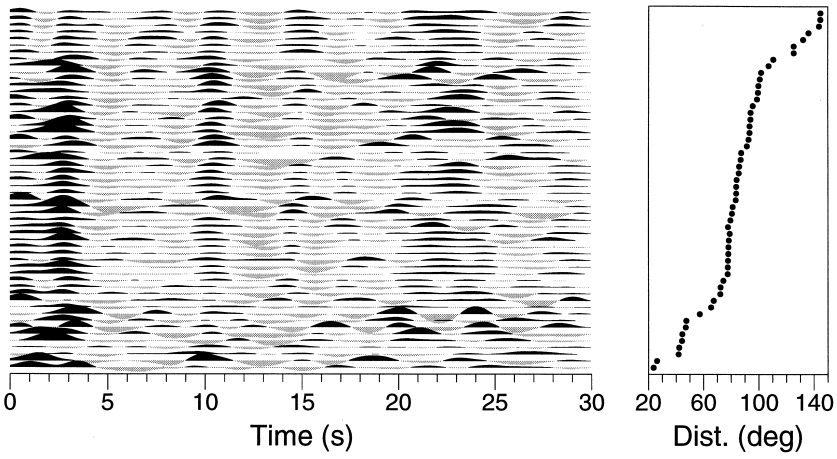

Figure 3. Same data as in Fig. 2, low-pass filtered at 3 s.

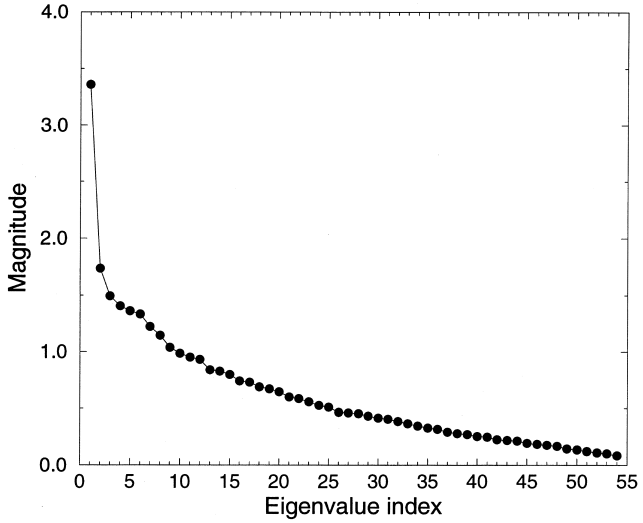

Figure 4. Magnitude of the eigenvalues associated with the data shown in Fig. 2.

these variations, which would also imply utilizing noisier eigenimages. This example demonstrates that SVD is mostly useful for filtering receiver functions from events that have nearly the same incidence angles because in this case the wave coherence is larger and the signal space is better reconstructed with a small number of eigenimages.

2.2.2 *Spectral matrix filtering*

Mari & Glangeaud (1990) introduced the SMF technique to process vertical seismic profiling data. They demonstrated that this technique is very efficient at separating upgoing and downgoing waves and isolating noise present in records. Nicollin (1991) also applied it with some success to explosion seismology data.

SMF operates in the frequency domain. Let $D_i(f)$ be the Fourier transform of the ith trace $\mathbf{d}_i$. The elements $S_{ij}(f)$ of the spectral matrix are formed with the cross-spectra of the different traces:

$$S_{ij}(f) = E[D_i(f) D_j^*(f)], \tag{3}$$

with E an estimation operator. In contrast to previous studies, we estimate the spectral matrix with a multitaper analysis technique, which we briefly describe [see Thomson (1982) and Park *et al.* (1987) for more details]. The $v^{(k)}(N, W)$ are the prolate eigentapers corresponding to the eigenvalues λ_k that quantify the fraction of energy contained within the frequency band $f \pm W$ (Park *et al.* 1987). The closer λ_k to 1, the less spectral leakage will affect the spectral estimates. We first determine the complex coefficients $y_{ik}(f)$ by taking the Fourier transform of the product of the trace $\mathbf{d}_i$ with $v^{(k)}(N, W)$:

$$y_i^{(k)}(f) = \sum_{t=0}^{N-1} v_t^{(k)} D_{i,t}\, \mathrm{e}^{i2\pi ft}. \tag{4}$$

The high-resolution estimate of the spectral matrix is then

$$S_{ij}(f) = \frac{1}{K} \sum_{k=0}^{K-1} \frac{y_i^{(k)}(f) y_j(k)^*(f)}{\lambda_k}, \tag{5}$$

where K is the number of tapers used.

Once the spectral matrix has been calculated, it is diagonalized:

$$\mathbf{S} = \sum_{i=1}^{R} \lambda_i \mathbf{v}_i \mathbf{v}_i^{\mathrm{T}}, \tag{6}$$

with R the rank of $\mathbf{S}$, $\mathbf{v}_i$ the ith eigenvector of $\mathbf{S}$ and λ_i the ith eigenvalue. The filtered section is then formed by projecting the vectors $\mathbf{D}_i$ on the first eigenvectors $\mathbf{v}_i$ of the spectral matrix:

$$D_{\mathrm{fil}} = \mathscr{F}^{-1}\left[\left(\sum_{i=1}^{n} \mathbf{D}_i \mathbf{v}_i^*\right)\mathbf{v}_i\right]. \tag{7}$$

In practice, n corresponds to the maximum value for which the residual data do not show any coherent signal. Usually, projecting the data on the first eigenvector is sufficient.

Fig. 6 shows the PRU section filtered by SMF, with $NW = 3$ and $K = 5$ and using the projection on the first eigenvector only. Globally, this method gives better results than SVD when filtering a set of receiver functions. The coherent part of the signal is clearly enhanced, and incoherent noise has been largely suppressed. The two phases at 3 and 10.5 s show the largest amplitudes but some other phases are also detected, with a positive polarity at 4.5, 5.5, 15 and around 23 s and a

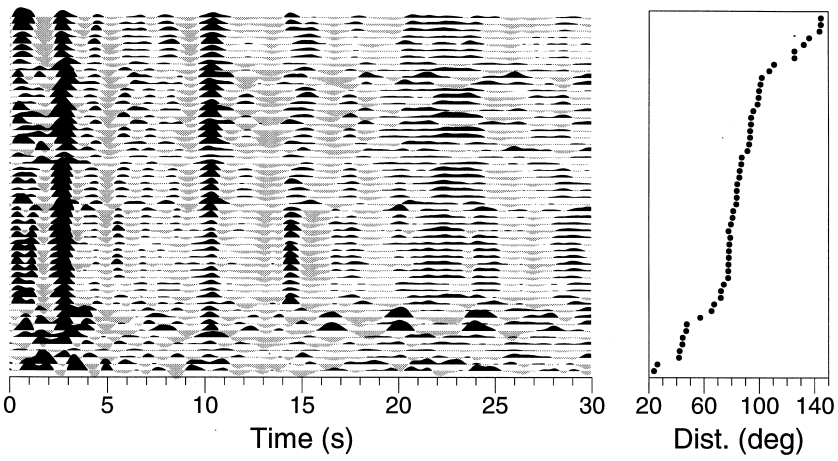

Figure 5. Data of Fig. 2, filtered by SVD. The reconstructed section is determined from the sum of the first six eigenimages.

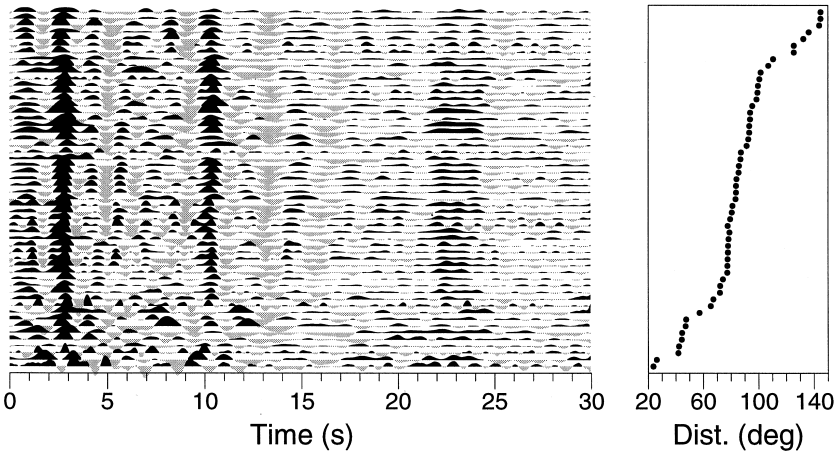

Figure 6. Data of Fig. 2, filtered by SMF. Data are projected on the first eigenvector of the spectral matrix.

negative polarity at 5, 13 and 16 s. The detection of the long-period phase around 23 s with both SVD (Fig. 5) and SMF (Fig. 6) is of special interest since this phase was almost completely hidden by a strong short-period noise in the initial data (Fig. 2).

The application of SVD and SMF to the PRU section demonstrates that it is possible to improve significantly the quality of receiver functions.

3 IDENTIFICATION OF REFLECTED AND CONVERTED WAVES AND DETERMINATION OF A SIMPLE CRUSTAL MODEL

Once detected, the different phases need to be identified. An important constraint in identifying the crustal phases shown in Fig. 1 comes from the existing relationships between their traveltimes. Let the traveltimes t_1 and t_2, the differential traveltimes between the conversion at the Moho and the P wave and between the first multiple and the P wave (see Fig. 1) respectively, be defined as

$$t_1 = t_{Pms} - t_P = \int_d^0 \left(\sqrt{\frac{1}{V_S^2} - p^2} - \sqrt{\frac{1}{V_P^2} - p^2} \right) dz \,, \tag{8}$$

$$t_2 = t_{PpPms} - t_P = \int_d^0 \left(\sqrt{\frac{1}{V_S^2} - p^2} + \sqrt{\frac{1}{V_P^2} - p^2} \right) dz \,. \tag{9}$$

The ratio R_t between t_2 and t_1 depends on the V_P/V_S ratio. From the measured R_t, it is thus possible to obtain a direct estimate of the crustal Poisson's ratio σ,

$$\sigma = \frac{1}{2}\left[1 - \frac{1}{R_V^2 - 1}\right], \tag{10}$$

that will slightly depend on the mean crustal velocity (Zandt & Ammon 1995; Zandt *et al.* 1995). The relationship between R_t and the V_P/V_S ratio considered by Zandt *et al.* (1995) and Zandt & Ammon (1995) can be further simplified when $p^2 \ll 1/V_P^2$. In this case, the mean V_P/V_S is simply given by

$$R_V = \frac{V_P}{V_S} \approx \frac{\frac{t_1}{t_2} + 1}{\frac{t_1}{t_2} - 1} = \frac{R_t + 1}{R_t - 1} \,. \tag{11}$$

For epicentral distances larger than 80°, relation (11) gives very accurate results. Ammon (1991) pointed out that when epicentral distance increases, the absolute amplitude of phases decreases because of the conversion coefficient decrease with decreasing incidence angle. Therefore, receiver functions corresponding to distant earthquakes are more likely to be dominated by noise. Indeed, the top 12 traces in the PRU section (Fig. 2) were determined from the analysis of events distant by more than 100°. For these events, the receiver functions are generated from the coda of the *PKP* phases. However, the noise amplitude on these traces is similar to that observed for closer events. All the coherent phases are also clearly visible, and no obvious artefacts generated by the triplication of the *PKP* phases are present. If the data selection is performed with care, it is thus possible to obtain reliable receiver functions in the 100°–140° epicentral distance range from the analysis of *PKP*.

As already mentioned, reflected and converted waves have respectively a negative and a positive apparent slowness relative to the P wave. This is easily seen by deriving eqs (8) and (9) with respect to the ray parameter p:

$$\frac{\partial \Delta t_1}{\partial p} = p \int_z^0 \left(\frac{1}{V_P^2} - p^2 \right)^{-\frac{1}{2}} - \left(\frac{1}{V_S^2} - p^2 \right)^{-\frac{1}{2}} dz > 0 \,, \tag{12}$$

$$\frac{\partial \Delta t_2}{\partial p} = -p \int_z^0 \left(\frac{1}{V_P^2} - p^2 \right)^{-\frac{1}{2}} - \left(\frac{1}{V_S^2} - p^2 \right)^{-\frac{1}{2}} dz < 0 \,. \tag{13}$$

Because $V_P > V_S$, the first derivative is always positive while the second derivative is always negative. For epicentral distances larger than 40°, the magnitude of the derivatives is very small, but for epicentral distances smaller than 40°, the effect of the differential slowness can be seen if the structure is simple enough and if the energy of scattered waves is small (see Fig. 6). This effect will be larger for large ray parameters. Therefore, selecting events with epicentral distances smaller than 30°, if possible, can provide additional constraints for the identification of waves. However, the processing of these events requires particular care because of the triplication of the P waves on the transition zone discontinuities, which complicates the deconvolution procedure. After processing, we found only two events in this distance range that could provide receiver functions of good quality.

Usually, the first 5 s of receiver functions are dominated by *P*-to-*S* conversions at crustal discontinuities. When a converted phase is detected, it is possible to look for the first multiple reflected at the top of the same discontinuity. Both phases should have the same polarity, comparable amplitudes and a traveltime ratio R_t given by eq. (11), using reasonable assumptions for R_V. For crustal rocks, measurements of R_V give values between 1.70 for granite–granodiorite and 1.86 for slate (Christensen 1996). This gives a ratio R_t between the traveltimes of the converted phase and the first multiple that ranges from 3.86 to 3.33. Similar relations can be used for other multiples. In particular, the differential traveltime between the second multiple (*PpSds*) and the first multiple (*PpPs*) is equal to the differential traveltime between the *Pds* converted phase and the *P* wave. For station PRU, the two prominent phases, at about 3.0 and 10.5 s are clearly related to the same discontinuity. The first is a conversion on a discontinuity at about 20 to 30 km depth (depending on the assumed mean velocity V_P and V_S in the crust) and the other is the first multiple associated with this discontinuity. The ratio between the two traveltimes gives $R_V = 1.77$ and $\sigma = 0.27$, which are a typical values for the crust of continental platforms (Zandt & Ammon 1995). Other phases are also visible but their amplitudes are lower. Of special interest is the arrival 15 s after the *P* wave. Unfortunately, this phase is not seen on the bottom traces corresponding to the smaller distances, probably because of a combination of scattering and interference with a phase with negative polarity. The real nature of this phase remains unclear. It may be either a conversion at a deep discontinuity (at about 140 km depth) or a crustal multiple. If this phase is a crustal multiple, then we expect to see a converted phase at about 4.5 s after the *P* wave. There is some evidence of such a phase for epicentral distances larger than 50° but this phase also seems to interfere with another phase with negative polarity that arrives slightly later. Therefore, no firm conclusion can be drawn regarding the shallow or deep origin of the 15 s phase. This point is further investigated in the next section

4 COMPARISON WITH THE RESULTS OF WAVEFORM INVERSION

Time-domain inversions are generally performed on stacks of receiver functions to retrieve the 1-D structure of the crust and upper mantle (Owens *et al.* 1984; Kosarev *et al.* 1993; Kind *et al.* 1995). These linearized inversions explore the model space in the vicinity of a starting model. The results are highly non-unique (Ammon *et al.* 1990) and strongly depend on both the starting model and the time window to be inverted. To illustrate this, the data of station PRU were inverted by assuming that the 15 s phase is either a conversion on an upper mantle discontinuity or a crustal multiple. Both inversions were performed on the stack of receiver functions corresponding to epicentral distances between 65° and 80°, for which the differences in incidence angles are negligibly small. The inversion method, introduced by Kosarev *et al.* (1993), is described in detail by Kind *et al.* (1995).

In the first inversion, the first 13 s after the *P*-wave arrival was inverted under the assumption that the 15 s phase is of mantle origin. The starting crustal model has a 1 km sediment layer over a simple gradient layer down to 23 km depth. Fig. 7 shows the inversion results and the waveform fits. The starting

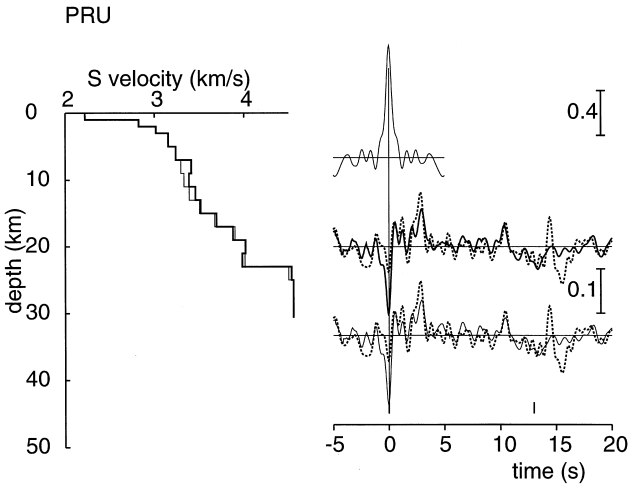

Figure 7. Results of the inversion for the first 13 s of the receiver functions determined for station PRU. The starting velocity model (thin line) and the final model (thick line) are plotted on the left. On the right, the upper trace shows the *P* waveform obtained after deconvolution and stacking. The bottom and middle traces show the synthetic waveforms corresponding to the starting model and the final model respectively, together with the observed *SV* component (dotted lines) after deconvolution and stacking.

model, plotted with a thin line, is close to the final model and both provide a very good fit to the observed first 13 s of the stacked *SV* component. The conversion at the Moho and the crustal multiples are the most prominent phases. As expected, a very simple crustal model is obtained that does not predict a strong arrival around 15 s.

In the second inversion, the first 18 s after the *P*-wave arrival was inverted. A starting model similar to the previous case was introduced for the upper 23 km, including a gradient layer representing the Moho at 35 km depth. The results of the inversion are shown in Fig. 8. The final model, obtained after three steps, is close to the initial model. The 15 s phase, strongly expressed in the data, corresponds to the first multiple on the Moho, while the conversion on the Moho itself is hardly

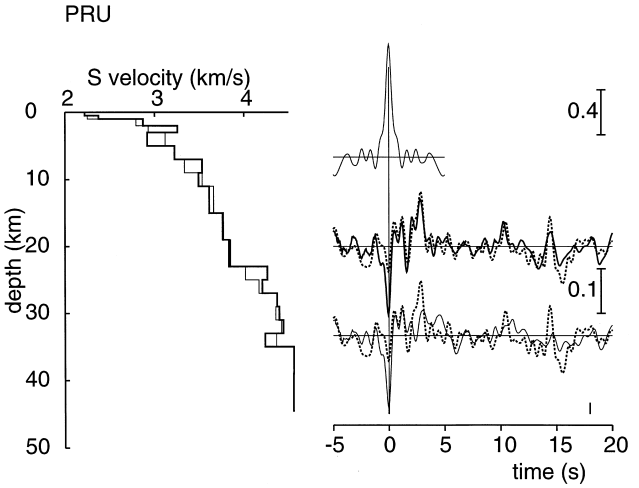

Figure 8. Results of the inversion for the first 18 s of the receiver functions determined for station PRU. Same plots as in Fig. 7.

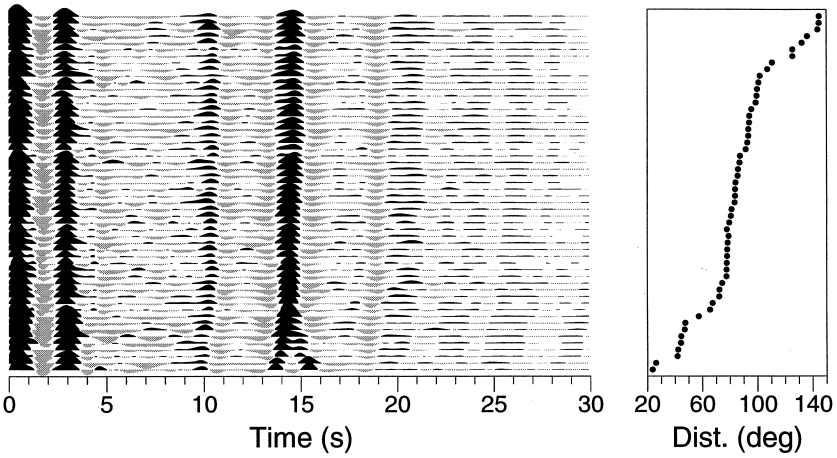

Figure 9. Radial components of the synthetic receiver functions computed in the final model of Fig. 8 with an additional discontinuity at 135 km depth.

seen because of interference with other crustal phases. Since the stacked waveforms are affected by scattering and lateral variations of the structure that are not taken into account in the forward modelling, the final model explains the data reasonably well with crustal structure only.

5 DISCUSSION

The example of station PRU demonstrates that the ambiguities in the identification of crustal phases remain even after waveform inversion. Thus, the seismic section interpretation should rely on other geophysical or geological constraints. Beránek & Zátopek (1981) reported a crustal thickness of about 35 km under station PRU, which was obtained by deep seismic sounding. This would suggest that the second model should be preferred. Moreover, Babuška & Plomerova (1992) determined the thickness of the lithosphere in Central Europe from an analysis of *P*-wave traveltime residuals. Their evaluation of the lithospheric thickness in the vicinity of station PRU is around 140 km. Therefore, the observed signal at 15 s might result from a superposition of a crustal multiple and a converted phase at 140 km depth. We have computed synthetic receiver functions in the second model with an additional discontinuity at 135 km depth. The synthetics were subsequently convolved with the longitudinal components of the seismograms and the result is shown in Fig. 9. From this simple model, which gives a reasonable fit of the stacked data, we are able to retrieve the main features of the observed seismic section, including the onset variations of the most prominent phases with epicentral distance. However, many coherent phases with small amplitudes observed in the data are not reproduced by this model. Another complexity of the PRU section is clearly seen in Fig. 10, where the data have been stacked in azimuthal windows and plotted as a function of backazimuth. Two coherent phases, at 1.5 and 4.5 s, are observed on the transverse components. These phases display a remarkable 360° periodic variation of their amplitudes. The phase at 3.5 s observed on the radial components also shows some systematic variations with respect to azimuth. These observations are easily explained by conversions at dipping interfaces (Chevrot 2000). The dip of the crustal layers is another source of bias when the waveform inversion is performed on a subset of receiver functions,

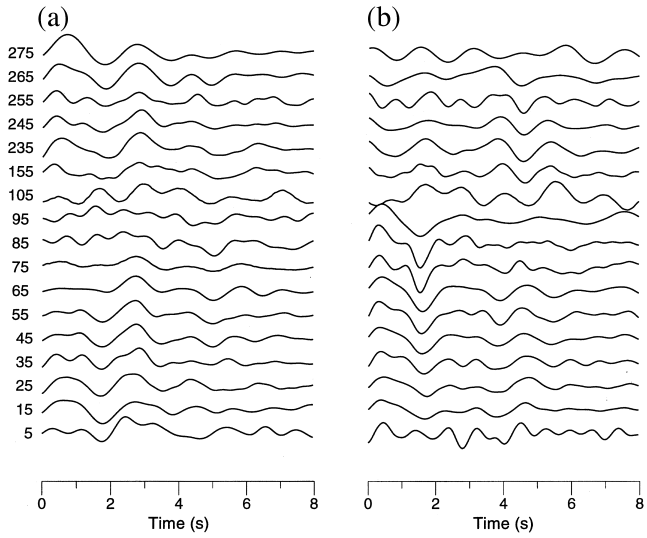

Figure 10. (a) Radial and (b) transverse components of the receiver functions for station PRU, stacked in azimuthal windows.

because 3-D structures are mapped into the final 1-D model. Obviously, much information is lost when the data are stacked, and the waveform inversion should be performed on the whole set of receiver functions. Improving the signal-to-noise ratio by SVD or SMF filtering would be an important factor for the success of this approach.

Our results emphasize the non-uniqueness of the models derived by a time-domain inversion of stacked receiver functions and their strong dependence on both the starting model and the time interval that is inverted. Shibutani *et al.* (1996) tried to overcome the problem of the choice of starting model by using a genetic algorithm inversion. In theory, this method explores the model space more efficiently, but the problem of the selection of the time interval to be inverted remains.

6 CONCLUSIONS

We have introduced new filtering techniques, singular value decomposition and spectral matrix filtering, to process receiver functions. We have shown that these techniques are very

efficient in improving the signal-to-noise ratio on individual receiver functions, to the point where it is possible to detect and identify crustal phases without stacking. Since the crust can be very heterogeneous, it is a clear advantage over the classical methods based on stacking, where the assumption that crustal phases arrive at the same time in every record is implicitly made.

Crustal phases are identified using their apparent slownesses and traveltimes with respect to the *P* wave. The identification of phases is easier from events with short epicentral distances (smaller than 40°) due to a larger separation in slowness. Additionally, the analysis of far earthquakes with epicentral distances larger than 80° allows a rapid and robust estimation of the mean V_P/V_S ratio in the crust from the traveltimes of *P*-to-*S* conversions at the Moho and the first multiple. Therefore, the typical 30°–90° epicentral distance range can be widened to a 20°–140° epicentral distance range. For most stations, this will significantly improve the azimuthal coverage, which is critical for anisotropy studies. Filtering techniques such as SVD and SMF help to detect weak arrivals. They are particularly attractive in processing the transverse components of seismograms, which are often very noisy but yet very important for constraining dipping interfaces and/or anisotropy (Levin & Park 1997b; Savage 1998). This important aspect is left for future studies.

ACKNOWLEDGMENTS

We are indebted to Dr Plomerova of the Geophysical Institute of Prague for her help in gathering information and seismic data. We thank the seismic data centre team from the Academy of Science of Prague (especially Jan Zednick) for the PRU data collection. We thank Grigoriy Kosarev for kindly making his receiver function inversion code available to us.

REFERENCES

Ammon, C.J., 1991. The isolation of receiver effects from teleseismic *P* waveforms, *Bull. seism. Soc. Am.,* 2504–2510.

Ammon, C.J., Randall, G.E. & Zandt, G., 1990. On the nonuniqueness of receiver function inversions, *J. geophys. Res.,* **95,** 15 303–15 318.

Babuška, V. & Plomerova, J., 1992. The lithosphere in Central Europe-seismological and petrological aspects, *Tectonophysics,* **20,** 141–163.

Beránek, B. & Zátopek, A., 1981. *Geophysical Syntheses in Czechoslovaquia,* Veda, Bratislava.

Bostock, M., 1997. Anisotropic upper-mantle stratigraphy and architecture of the Slave craton, *Nature,* **390,** 392–395.

Bostock, M., 1998. Mantle stratigraphy and evolution of the Slave province, *J. geophys. Res.,* **103,** 21 183–21 200.

Burdick, L.J. & Langston, C.A., 1977. Modeling crustal structure through the use of converted phases in teleseismic body waveforms, *Bull. seism. Soc. Am.,* **67,** 677–691.

Cassidy, J.F., 1992. Numerical experiments in broadband receiver function analysis, *Bull. seism. Soc. Am.,* **82,** 1453–1474.

Chevrot, S., 2000. Multichannel analysis of shear wave splitting, *J. geophys. Res.,* submitted.

Chevrot, S., Vinnik, L. & Montagner, J.P., 1999. Global scale analysis of the mantle *Pds* phases, *J. geophys. Res.,* **104,** 20 203–20 219.

Christensen, N.I., 1996. Poisson's ratio and crustal seismology, *J. geophys. Res.,* **101,** 3139–3156.

Durrheim, R.J. & Mooney, W.D., 1991. Archean and Proterozoic crustal evolution: evidence from crustal seismology, *Geology,* **19,** 606–609.

Freire, S.L.M. & Ulrych, T.J., 1988. Application of singular value decomposition to vertical seismic profiling, *Geophysics,* **53,** 778–785.

Glangeaud, F. & Mari, J.L., 1994. Wave separation, *Rev. Inst. Français Pétrole,* **49,** 1–75.

Kind, R., Kosarev, G.L. & Petersen, N.V., 1995. Receiver functions at the stations of the German Regional Seismic Network, *Geophys. J. Int.,* **121,** 191–202.

Kosarev, G.L., Makeyeva, L.I. & Vinnik, L.P., 1984. Anisotropy of the mantle inferred from observations of *P* to *S* converted waves, *Geophys. J. R. astr. Soc.,* **76,** 209–220.

Kosarev, G.L., Petersen, N.V., Vinnik, L.P. & Roecker, S.W., 1993. Receiver functions for the Tien Shan analog broadband network: contrasts in the evolution of structures across the Talasso-Fergana fault, *J. geophys. Res.,* **98,** 4437–4448.

Langston, C.A., 1979. Structure under Mount Rainier, Washington, inferred from teleseismic body waves, *J. geophys. Res.,* **84,** 4749–4762.

Levin, V. & Park, J., 1997a. Crustal anisotropy in the Ural mountains foredeep from teleseismic receiver functions, *Geophys. Res. Lett.,* **24,** 1283–1286.

Levin, V. & Park, J., 1997b. *P-SH* conversions in a flat-layered medium with anisotropy of arbitrary orientation, *Geophys. J. Int.,* **131,** 253–266.

Mari, J.L. & Glangeaud, F., 1990. Spectral matrix filtering applied to VSP processing, *Rev. Inst. Français Pétrole,* **45,** 417–434.

McNamara, D.E. & Owens, T.J., 1993. Azimuthal shear wave velocity anisotropy in the Basin and Range province using moho *Ps* converted phases, *J. geophys. Res.,* **98,** 12 003–12 017.

Nicollin, F., 1991. Spectral matrix filtering applied to explosion seismology data: examples from the Western Alps, *Tectonophysics,* **195,** 299–309.

Owens, T.J. & Crosson, R.S., 1988. Shallow structure effects on broadband teleseismic *P* waveforms, *Bull. seism. Soc. Am.,* **78,** 96–108.

Owens, T.J. & Zandt, G., 1985. The response of the continental crust-mantle boundary observed on broadband teleseismic receiver functions, *Geophys. Res. Lett.,* **12,** 705–708.

Owens, T.J., Zandt, G. & Taylor, S.R., 1984. Seismic evidence for an ancient rift beneath the Cumberland plateau, Tenessee: a detailed analysis of broadband teleseismic *P* waveforms, *J. geophys. Res.,* **89,** 7783–7795.

Park, J., Lindberg, C.R. & Vernon, F.L., 1987. Multitaper spectral analysis of high-frequency seismograms, *J. geophys. Res.,* **92,** 12 675–12 684.

Savage, M.K., 1998. Lower crustal anisotropy or dipping boundaries? Effects on receiver functions and a case study in New Zealand, *J. geophys. Res.,* **103,** 15 069–15 087.

Shibutani, T., Sambridge, M. & Kennett, B., 1996. Genetic algorithm inversion for receiver functions with application to crust and uppermost mantle structure beneath eastern australia, *Geophys. Res. Lett.,* **23,** 1829–1832.

Thomson, D.J., 1982. Spectrum estimation and harmonic analysis, *Proc. IEEE,* **70,** 1055–1096.

Vinnik, L., 1977. Detection of waves converted from *P* to *SV* in the mantle, *Phys. Earth planet. Inter.,* **15,** 39–45.

Yuan, X., Ni, J., Kind, R., Mechie, J. & Sandvol, E., 1997. Lithospheric and upper mantle structure of southern Tibet from a seismological passive source experiment, *J. geophys. Res.,* **102,** 27 491–27 500.

Zandt, G. & Ammon, C.J., 1995. Continental crust composition constrained by measurements of crustal Poisson's ratio, *Nature,* **374,** 152–154.

Zandt, G., Myers, S.C. & Wallace, T.C., 1995. Crust and mantle structure across the Basin and Range-Colorado plateau boundary at 37 degrees N latitude and implications for Cenozoic extensional mechanism, *J. geophys. Res.,* **100,** 10 529–10 548.